PNAS Nexus, 2025, 4, pgaf058
https://doi.org/10.1093/pnasnexus/pgaf058
Advance access publication 24 February 2025
Research Report

Atmospheric sulfate aerosol formation enhanced by interfacial anions

Gehui Wang[a,*,1], Si Zhang[a,1], Can Wu[a,*], Tong Zhu[b], Xinbei Xu[a], Shuangshuang Ge[a], Haitao Sun[c], Zhenrong Sun[c], Jiaxin Wang[d], Yuemeng Ji[d], Jian Gao[e], Yanqin Ren[e], Hong Li[e], Fang Zhang[f], Yuan Wang[g] and John H. Seinfeld[h]

[a]School of Geographic Sciences, Key Lab of Geographic Information Science of the Ministry of Education, East China Normal University, Shanghai 200241, China
[b]School of Chemistry and Molecular Engineering, East China Normal University, Shanghai 200241, China
[c]State Key Laboratory of Precision Spectroscopy, School of Physics and Electronic Sciences, East China Normal University, Shanghai 200241, China
[d]School of Environmental Science and Engineering, Guangdong University of Technology, Guangzhou 510006, China
[e]State Key Laboratory of Environmental Criteria and Risk Assessment, Chinese Research Academy of Environmental Sciences, Beijing 100012, China
[f]School of Civil and Environmental Engineering, Harbin Institute of Technology (Shenzhen), Shenzhen 518055, China
[g]Department of Earth System Science, Stanford University, Stanford, CA 94305, USA
[h]Division of Chemistry and Chemical Engineering, California Institute of Technology, Pasadena, CA 91125, USA
*To whom correspondence should be addressed: Email: ghwang@geo.ecnu.edu.cn (G.W.); Email: cwu@geo.ecnu.edu.cn (C.W.)
[1]G.W. and S.Z. contributed equally to this work.
Edited By Dennis Hartmann

Abstract

Heterogeneous oxidation of SO_2 by NO_2 on aerosols has recently been found to be one of the major formation pathways of sulfate in the polluted troposphere, but the chemical mechanisms and kinetics remain uncertain. By combining lab experiments, theoretical chemistry calculations, and field measurements, here we show that the SO_2 oxidation by NO_2 is critically dependent on anions at the air–aerosol aqueous interface. The reaction rate of NO_2 with HSO_3^- (1.1×10^8–1.6×10^9 M^{-1} s^{-1}) is more than four orders of magnitude larger than the traditionally held value for the bulk phase due to the abundant occurrence of chloride, nitrate, and carboxylic anions at the air–aqueous interface, which remarkably accelerates sulfate formation during China haze periods by enhancing the uptake of NO_2 through interfacial electrostatic attraction. Atmospheric models not accounting for this aerosol interfacial process likely produce major misrepresentations of tropospheric sulfate aerosols under polluted conditions.

Keywords: air pollution, China haze, sulfate aerosols, interface chemistry, aerosol kinetics

Significance Statement

A high level of sulfate still frequently occurs in haze periods in China, but the formation mechanism remains unclear. From atmospheric measurement in Beijing, laboratory experiments, and quantum chemical simulation, we show that the heterogeneous oxidation of SO_2 by NO_2 in aerosol aqueous phase is the predominant pathway of sulfate formation during Chinese haze periods, which is significantly enhanced by anions at the air–aqueous interface through an electrostatic attraction with NO_2. Our work reveals that air–aqueous interfacial chemistry is a key role in secondary aerosol formation in real atmosphere and should be accounted for models.

Introduction

Sulfate is one of the major components of atmospheric aerosols and profoundly affects climate, human health, and the environment (1–3). Tropospheric sulfate is largely formed from heterogeneous reactions of SO_2 with oxidants such as O_3, H_2O_2, and O_2 catalyzed by transition metal ions (TMIs, mainly Fe^{3+} and Mn^{2+}) in aerosols, fogs, and cloud droplets (2, 4–7). However, the rapid formation of sulfate in China haze periods has often been underestimated by numerical models, suggesting some unknown sulfate formation mechanisms (8, 9). Recently, a few studies have proposed that heterogeneous oxidation of SO_2 by NO_2 with neutralization by NH_3 under humid conditions is a major formation pathway of sulfate during winter haze periods in China (1, 7, 10–16), but these studies are controversial regarding the role of NO_2 in the SO_2 oxidation process. Some researchers have proposed that the oxidation of SO_2 by NO_2 in the aerosol aqueous phase produces sulfate and HONO, and HONO subsequently evaporates into the gas phase (Eqs. 1 and 2) (1, 7, 17). In contrast, others presume that the dissolved SO_2 is oxidized into SO_4^{2-} not only by NO_2 (Eq. 1) but also by NO_2^-, and the latter is reduced into N_2O and subsequently evaporates into the gas phase (Eq. 3) (10, 13, 18). Such controversial results suggest that some

Competing Interest: The authors declare no competing interests.
Received: November 29, 2024. **Accepted:** February 10, 2025

fundamental processes governing the reaction of SO_2 with NO_2 in the troposphere are still not understood. Therefore, revealing the mechanisms and kinetics is necessary because SO_2, NO_x, and their secondary products, e.g. sulfate, nitrate, and ozone, are the major pollutants in the troposphere.

$$2NO_2(aq) + S(IV)(aq) + H_2O \rightarrow 2H^+(aq) + 2NO_2^-(aq) + S(VI)(aq) \quad (1)$$

$$H^+(aq) + NO_2^-(aq) \rightarrow HONO(g) \quad (2)$$

$$2NO_2^-(aq) + 2S(IV)(aq) \rightarrow N_2O(g) + 2S(VI) \quad (3)$$

$$2NO_2 + H_2O(aq) \rightarrow HONO + HNO_3 \quad (4)$$

To date, studies on the heterogeneous formation of sulfate through SO_2 oxidation in aerosols, fogs, and clouds have only focused on the reaction processes in the bulk phase and deemed that the bulk-phase acidity (pH) is a crucial factor controlling the SO_2 oxidation pathways and sulfate production in the global atmosphere (10, 14, 19–22). In the past decade, a number of studies have found that ion distributions at the air–water interface of an electrolyte solution are different from those in the bulk phase. Some polarizable anions, such as Cl^-, Br^-, I^-, NO_3^-, and HCO_3^-, preferably stay near the most top surface, while some cations, such as Na^+ and Ca^{2+}, and divalent anions, such as SO_4^{2-} and CO_3^{2-}, stay near the bulk phase (23–26). Such different distributions can result in anions being enriched in the air–aqueous interface (27, 28), and thus may significantly affect the reactions of gaseous pollutants with atmospheric aerosols, fogs, and cloud droplets. However, direct field evidence on such an interfacial effect is lacking, and thus, the involved atmospheric reactions are unknown because compositions of the air–aqueous interface in the atmosphere cannot be measured directly.

Here, we used a laboratory smog chamber (Fig. S1) to mimic the impact of the air–aqueous interfacial ions on the heterogeneous oxidation of SO_2 by NO_2 in preexisting aerosols during haze periods in China by exposing a series of inorganic and organic seeds to SO_2, NO_2, and NH_3 under humid conditions. Both gas- and aerosol-phase species were comprehensively monitored online by using a series of sophisticated instruments and simulated by using state-of-the-art molecular dynamics (MD) models and quantum chemical calculations to explore the reaction process of SO_2 with NO_2. Based on the field observations, laboratory chamber experiments, and MD simulations, we found a key role of air–aqueous interfacial anions in sulfate formation process in Beijing by investigating the winter haze chemistry.

Results

Distinct behavior of SO_2 oxidation at the air–aqueous interface

To investigate the heterogeneous oxidation of SO_2 by NO_2 on preexisting aerosols in urban atmosphere, we exposed different types of seeds on a polydisperse mode including NaCl, NH_4NO_3, $(NH_4)_2SO_4$, a mixture of $(NH_4)_2SO_4$ and NaCl, oxalic acid, and sucrose, which are typical components of tropospheric aerosols (29, 30), to the same levels of SO_2 (600 ppb), NO_2 (600 ppb), and NH_3 (80 and 190 ppb) under 90% relative humidity (RH) conditions, respectively. All the seed solution was added with ethylenediaminetetraacetic acid (EDTA) before being nebulized into the chamber to remove a possible impact of TMIs. Figure 1 shows the

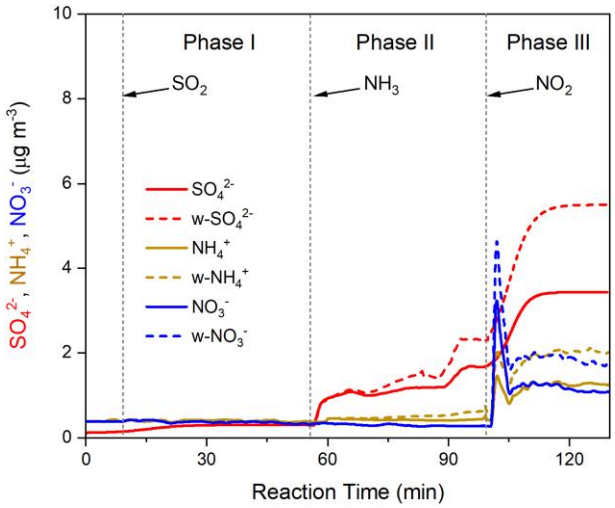

Fig. 1. Changes in compositions of particles in the chamber during the exposure of NaCl seeds to SO_2, NH_3, and NO_2 under 90% RH conditions. The figure shows the time evolution of aerosol-phase (SO_4^{2-}, NH_4^+, NO_3^-, and wall-loss-corrected SO_4^{2-} (w-SO_4^{2-}), NH_4^+ (w-NH_4^+), and NO_3^- (w-NO_3^-) species for a typical NaCl aerosol seed experiment under 80 ppb NH_3 (g) conditions. w-SO_4^{2-}, w-NH_4^+, and w-NO_3^- concentrations were derived by correcting SO_4^{2-}, NH_4^+, and NO_3^- concentrations using a wall-loss rate before adding NH_3 into the chamber (see Materials and methods for more details).

variations in concentrations of sulfate, nitrate, and ammonium in the chamber during the exposure of NaCl seeds. When SO_2 was introduced, a very small amount of sulfite was formed on the NaCl seeds (phase I in Fig. 1). The sulfate increased to about 1.5 μg m^{-3} after NH_3 was introduced (phase II in Fig. 1). Such a small amount of sulfate formed in the absence of NO_2 is most likely caused by a reaction between SO_2 and impurities of peroxides in the solution and the increased dissolved S(IV) (15). After NO_2 was further introduced, S(IV) was oxidized into S(VI) and a sharp increase of 4.0 μg m^{-3} sulfate was detected (phase III in Fig. 1), suggesting a rapid formation of sulfate on the NaCl seeds via heterogeneous oxidation of SO_2 by NO_2. The reactive uptake coefficients of SO_2 in the three stages were 2.5×10^{-7} (unary uptake, SO_2 only, phase I in Fig. 1), 1.5×10^{-6} (co-uptake, SO_2 and NH_3, phase II in Fig. 1), and 2.6×10^{-5} (trinary uptake, SO_2, NH_3, and NO_2, phase III in Fig. 1), respectively, indicating an enhanced interaction of SO_2 with NO_2 in the presence of NH_3. Such a SO_2 uptake was greater under 190 ppb NH_3 conditions (Tables S1 and S2), because NH_3 reduces the aerosol acidity and makes more S(IV) available at the interface. Similar results were also observed for oxalic acid, NH_4NO_3, and $(NH_4)_2SO_4$/NaCl mixture seeds, respectively (Fig. S2A–C, and Tables S1 and S2). However, no additional sulfate was formed on either $(NH_4)_2SO_4$ or sucrose seeds during the exposure (Fig. S2D and E). Such distinct differences in sulfate formation should be ascribed to the properties of seeded particles rather than the addition of EDTA into the seeds, because all the seeds contained the same amount (2 mM) of EDTA. Figure S3 compares the sulfate production rate on NaCl seeds with a different size. It can be seen that both γ, which is the uptake coefficient of SO_2, and $R_{SO_4^{2-}}$/SA, which is the sulfate formation rate ($R_{SO_4^{2-}}$) normalized by the surface area (SA) of seeds, are ~50% higher on NaCl seeds with a 60-nm diameter than on NaCl seeds with a 100-nm diameter. Such a dependence of sulfate production rate on seed particle size is in agreement with the experimental results reported by Liu and Abbatt (15) and suggests

that the heterogeneous oxidation of SO_2 by NO_2 proceeds at the aerosol surface.

On the contrary to the traditional Debye–Hückel theory of bulk aqueous electrolytes, a number of studies found that in the air–water interface of an electrolyte solution, some polarizable ions, such as halogen ions (Cl^-, Br^-, and I^-), NO_3^-, HCO_3^-, carboxylate, and NH_4^+, stay closer to the surface, while other ions, such as Na^+, K^+, SO_4^{2-}, and CO_3^{2-}, stay deeper in the bulk phase (31, 32). Thus, the air–aqueous interfaces of wetted NaCl and oxalate seeds are enriched with anions, while that of $(NH_4)_2SO_4$ seeds are enriched with cations. We assume that the anions at the air–aqueous interface of an aerosol may greatly promote the transport of NO_2 from the gas phase into the aqueous phase and thus enhance SO_2 oxidation by NO_2. To elucidate this effect, we used an MD model to simulate the distribution of ions in a NaCl solution droplet with a concentration (2 M NaCl) similar to that in our chamber experiments (33). As shown in Fig. 2A, Na^+ has a high distribution at a distance of ~11 Å from the water surface, while Cl^- has the largest distribution at a distance of ~8 Å from the water surface, which means that Cl^- ions are more accessible to the air–aqueous surface (34). At deeper positions, the concentrations of both ions are nearly the same (Fig. 2A). The layered Na^+ and Cl^- can form an electric field directed toward the water surface, which is the same as the direction of the dipole moment of NO_2 and thus efficiently promotes the adsorption of NO_2. When NO_2 moves from the air to the surface of the water slab, it may even directly collide with Cl^- ions at the surface (Fig. 2B). Figure 2C shows the electrostatic potential of the NO_2–Cl^- interaction calculated by the quantum chemical method. It can be seen that the negatively charged Cl^- ion has a strong attraction to the partially positively charged N atom. In fact, a σ bond could be formed between the single unoccupied molecular orbital (SUMO) of NO_2 and the highest occupied molecular orbital (HOMO) of Cl^- (Fig. 2B), which therefore significantly enhances NO_2 uptake by the wetted NaCl aerosols.

Because at the air–water interface of a solution NH_4^+ ions preferably stay near the surface with the counterpart SO_4^{2-} ions locating deeper in the bulk phase (35, 36), and sucrose is a nonionizable organic compound, the air–water interfaces of $(NH_4)_2SO_4$ and sucrose seeds in the chamber lack anions. Therefore, NO_2 molecules cannot effectively dissolve into the aerosol aqueous phase due to their poor solubility (2). As a result, SO_2 cannot be efficiently oxidized by NO_2, and thus, no sulfate was formed on $(NH_4)_2SO_4$ and sucrose seeds unless NaCl was added to the $(NH_4)_2SO_4$ solution (Fig. S2C–E). Hua et al. (37) found that NO_3^- is more accessible than NH_4^+ to the air–water surface. Mahiuddin et al. (38) investigated the surface behavior of aqueous solutions of diacids, including oxalic acid using MD model, and found all these acids exhibit a significant propensity for the air–water interface. Enami et al. (39) later reported that dicarboxylic acids at the surface largely exist as monoanion and undissociated forms. Thus, like NaCl seeds, the air–aqueous interface of NH_4NO_3 and oxalic acid seeds is also enriched with anions, which effectively trapped NO_2 and resulted in a rapid formation of sulfate after NO_2 was introduced (Fig. S2B, and Tables S1 and S2).

Oxidation pathway of SO_2 by NO_2

To clarify the oxidation pathway of SO_2 by NO_2, we exposed NaCl seeds to NO_2, SO_2, and NH_3 in an order being different from that in Fig. 1. As seen in Fig. S4, at phase I, NO_2 molecules disproportionate on the wetted seeds (Eq. 4) (40, 41), thus, ~8.0 μg m^{-3} of NO_3^- in the chamber was detected. After SO_2 was added into the chamber, the heterogeneous oxidation of SO_2 with NO_2 proceeded at the air–aqueous interface of the NaCl seeds. At this moment, only a small amount of sulfate was detected (Fig. S4, phase II), because the particles became very acidic due to the formation of sulfuric acid, which prevented further dissolution of SO_2 and thus limited the availability of S(IV). After NH_3 was introduced into the chamber, both SO_4^{2+} and NH_4^+ significantly increased due to the neutralization of NH_3 (Fig. S4, phase III), but NO_3^- concentration was almost constant as that in phase I, suggesting that NH_3 may accelerate NO_2 hydrolysis rate (42) but does not change the reaction equilibrium. During the whole process, no N_2O or NO was produced. Moreover, after SO_2 and NH_3 were injected into the chamber, the increase in HONO concentration was stoichiometrically equal to the decreased NO_2 concentration in the absence and presence of NaCl seeds (Fig. S5). These results clearly show that Eqs. 1 and 2, rather than Eq. 3, are the reaction pathways of SO_2 oxidation by NO_2. The ISORROPIA-II thermodynamic model calculation results show that the pH values of NaCl particles in the chamber after the reaction were ~5.0 (Tables S1 and S2). Our previous work revealed that under such moderate acidic conditions, the gas-phase HONO(g) concentration in the chamber is 2–3 orders of magnitude higher than that in the aerosol liquid phase due to the high volatility of HONO and the high specific SA of aerosols (17). Therefore, in the chamber, the HONO formed in the aerosol aqueous phase quickly evaporated into the gas phase, resulting in very minor amounts of HONO and NO_2^- remaining in the aqueous phase (17). Consequently, oxidation of S(IV) by dissolved HONO (aq) or NO_2^- was negligible, and no N_2O(g) in the chamber was detected (Fig. S4).

To further clarify the reaction pathway of SO_2 with NO_2 in the aerosol aqueous phase, we carried out a computational study to investigate the reactions of SO_2 and NO_2 in water by using density functional theory (43–45) and compare the NO_2 disproportionation pathway with the redox between NO_2 and SO_2 (HSO_3^-). As shown in Fig. 3, the pathway of disproportionation starts from a NO_2 dimer, in which the optimal pathway has a six-membered ring transition state TS4 as the rate-determining state. Relative to a NO_2 dimer, TS4 requires a 10.7-kcal mol^{-1} activation free energy. Alternatively, at higher concentration, the disproportionation pathway can start from the most stable N_2O_4, which has a lower Gibbs free energy of −4.9 kcal mol^{-1}, making the pathway behave as a first order reaction with an activation Gibbs free energy of 15.6 kcal mol^{-1}. For the pathway of NO_2 reduction by HSO_3^-, one NO_2 molecule and one HSO_3^- ion can be connected via hydrogen bonding with solvent water, forming intermediate IM1. An asynchronous concerted dual hydrogen atom transfer process can smoothly connect IM1 to IM2 via TS1. Relative to the substrate, TS1 has a Gibbs free energy of 8.0 kcal mol^{-1}, which is 2.7 kcal mol^{-1} lower than that of NO_2 disproportionation, approximately corresponding to a 100-fold difference in conversion rate of NO_2. Through TS1, one molecule HONO and a SO_3^- radical anion were generated, which are still connected through a water molecule. After IM2 formation, another molecule of NO_2 radical can readily react with SO_3^- radical through radical–radical coupling. This process is barrierless and highly spontaneous, giving the S–O-bonded intermediate IM3. IM3 can then react with water through a six-membered ring transition state TS3 to give IM4, which subsequently dissociate into HSO_4^- and another molecule of HONO.

Kinetics of SO_2 oxidation by NO_2

In the chamber, pH values of the aqueous phase of seed particles are 3.5–5.0 (Tables S1 and S2), which are similar to those observed

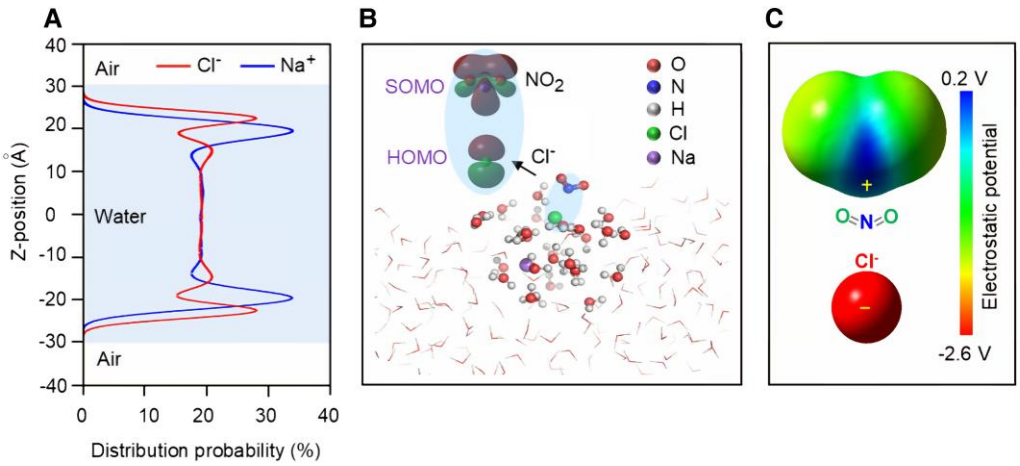

Fig. 2. Multiscale simulations of the NO_2-Cl^- interaction at the air–aqueous interface. A) MD simulation of the distribution of ions at the air–water interface of a 2-M NaCl solution (the simulation was run in the NVT (NVT is the canonical ensemble, which is a statistical mechanism state distribution where the number of particles (N), volume (V) and temperature (T) are constant) ensemble for 200 ns, and the system temperature was kept at 298 K). B) A typical snapshot of the absorption of NO_2 on a wetted NaCl aerosol. The frontier orbitals of Cl^- HOMO and NO_2 SUMO were also calculated. C) Electrostatic potential distributions of NO_2 and Cl^-.

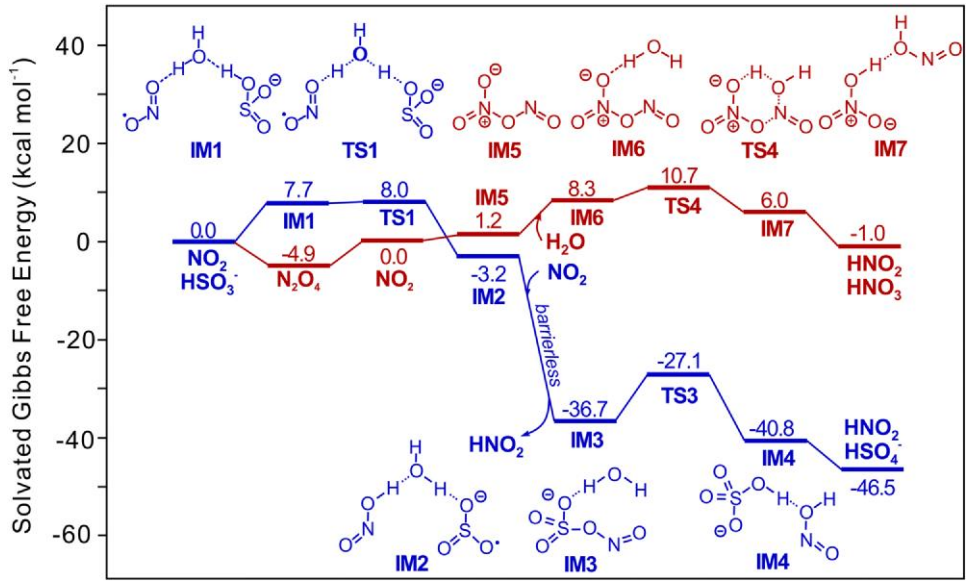

Fig. 3. Reaction pathways of NO_2 with HSO_3^- and NO_2 disproportionation. All energies labeled are the Gibbs free energy calculated at the PBE0-D3/def2-TZVPD level with SMD solvation in water.

in Beijing winter haze periods (Table S3). Under such moderate acidic conditions, NO_2 reacts mostly with HSO_3^- rather than SO_3^{2-} (2, 46). Thus, the formation rate of sulfate can be expressed as follows (see the details in SI Appendix S1):

$$\frac{d[SO_4^{2-}]}{dt} = \left(\frac{k_{NO_2^+HSO_3^-}}{[H^+]}\right) k_{a1} H_{SO_2} P_{SO_2} H_{NO_2} P_{NO_2} \quad (5)$$

where $d[SO_4^{2-}]$ is the molar concentration of sulfate during the reaction time of dt. $k_{NO_2^+HSO_3^-}$ is the reaction rate constant of Eq. 1. $[H^+]$ is the molar concentration of hydrogen ions in the aqueous phase of seed particles, which was calculated by using the ISORROPIA-II model. k_{a1} is the dissociation constant of HSO_3^-. H_{SO_2} and H_{NO_2} are the Henry's law constants of SO_2 and NO_2. P_{SO_2} and P_{NO_2} are the averaged partial pressures of SO_2 and NO_2 in the chamber during the reaction time of dt (2, 15).

$$k_{exp} = \frac{(d[SO_4^{2-}])/dt}{k_{a1} H_{SO_2} P_{SO_2} H_{NO_2} P_{NO_2}} = \frac{k_{NO_2^+HSO_3^-}}{[H^+]} \quad (6)$$

$$k_{NO_2^+HSO_3^-} = k_{exp}\,[H^+] \quad (7)$$

Based on the Eq. 5, the total reaction rate k_{exp} of SO_2 with NO_2 in the chamber, i.e. Eq. 6, can be further expressed as the Eq. 7. By plotting a log–log relationship of k_{exp} with $[H^+]$, we found that k_{exp} robustly linearly correlated with hydrogen ion activity during the reaction of SO_2 with NO_2 in the chamber with a slope of −1 ($R^2 = 0.77$, Fig. 4), again demonstrating that the reaction of

NO_2 with HSO_3^- rather than with SO_3^{2-} is the dominant formation pathway of sulfate in the chamber. We further calculated the effective rate constant $k_{NO_2^+HSO_3^-}$ of oxidation of SO_2 by NO_2 in the chamber by using the Eq. 7 (2, 15). As seen in Tables S1 and S2, $k_{NO_2^+HSO_3^-}$ values ranged from 1.1×10^8 to 1.6×10^9 $M^{-1}s^{-1}$ under the two levels of NH_3 conditions, which are over 4 orders of magnitude higher than those (1.5×10^4–1.4×10^5 $M^{-1}s^{-1}$) obtained for bulk solutions (46, 47), further revealing that SO_2 oxidation by NO_2 is enhanced by anions at the air–aqueous interface.

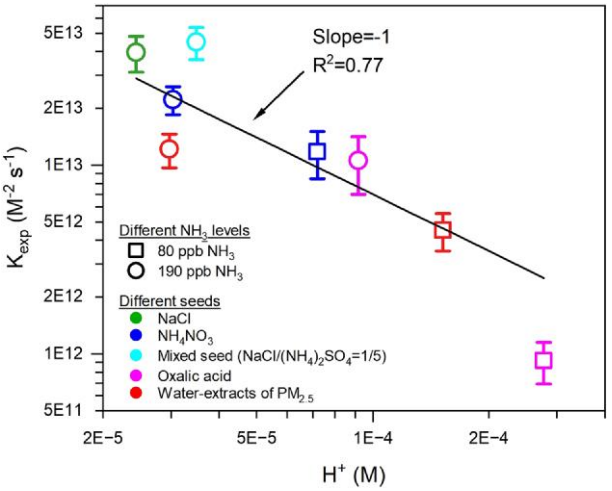

Fig. 4. K_{exp} as a function of hydrogen ion activity.

Discussion

To recognize whether such an interfacial effect is important for sulfate formation in the real troposphere, we investigated the aerosol chemistry in Beijing, China, during winter 2018. As shown in Fig. S6, the daily concentration of $PM_{2.5}$ in Beijing during the campaign frequently exceeded 75 μg m^{-3}, the second grade National Air Quality Standard, among which two heavy haze events occurred in the city with a daily $PM_{2.5}$ level >200 μg m^{-3}. During the two haze events, sulfate sharply increased to 20 and 39 μg m^{-3} (Fig. 5A, Table S3), with an uptake coefficient (γ_{SO_2}) of SO_2 of $7.0\pm1.2\times10^{-5}$ in Haze I and $9.5\pm0.2\times10^{-5}$ in Haze II (Table S4), indicating an efficient heterogeneous oxidation of SO_2. The sum of the concentrations of NO_3^- and Cl^- accounted for 20 and 17% of $PM_{2.5}$ in the two haze periods. In addition, over 0.3 μg m^{-3} oxalic acid in $PM_{2.5}$ was detected in Beijing during the Haze II event (Fig. 5B). We assumed that these abundant chloride, nitrate, and carboxylic anions accumulated in the air–aqueous interface of aerosols in the haze development process and resulted in the rapid formation of sulfate by enhancing the uptake of NO_2.

To corroborate the above assumption, we mimicked sulfate formation in Beijing during haze episodes by exposing particles that had been atomized from water extracts of $PM_{2.5}$ samples

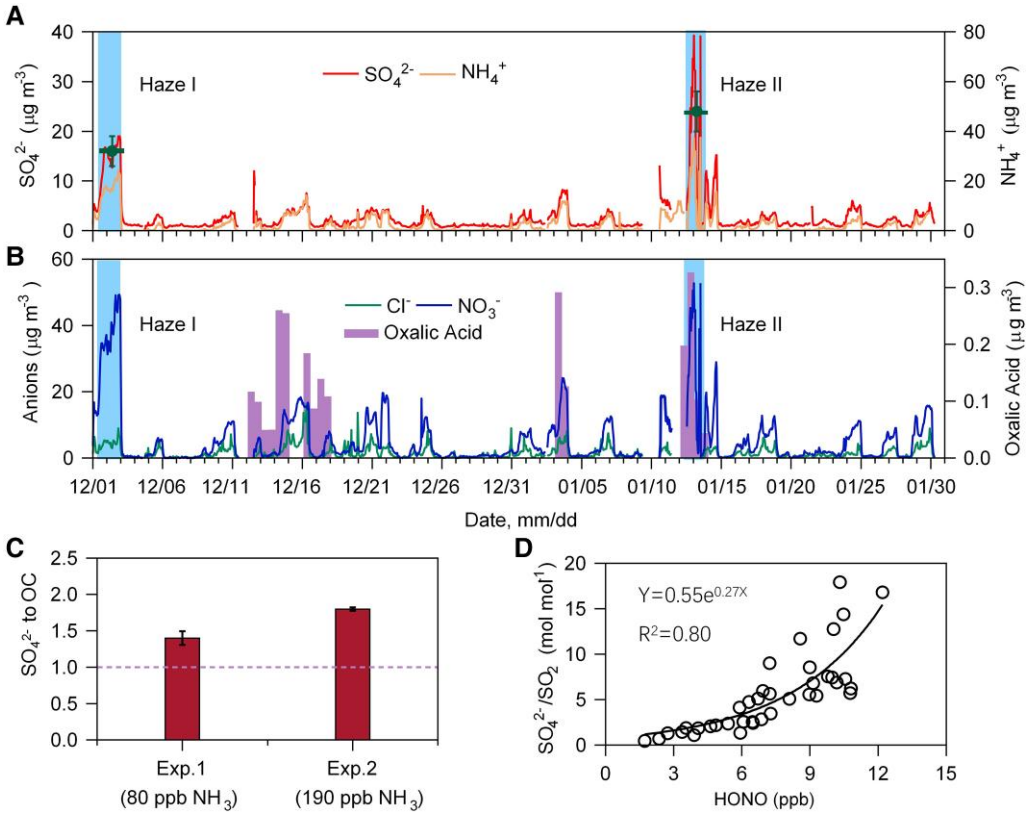

Fig. 5. Sulfate formation in China haze episodes. A and B) Temporal variations in the concentrations of NH_4^+, SO_4^{2-}, NO_3^-, Cl^-, and oxalic acid in $PM_{2.5}$ in Beijing during the 2018 winter campaign. Blue shadows indicate a haze event with a daily $PM_{2.5}$ larger than 200 μg m^{-3}, and the short lines in (A) are the average concentrations of SO_4^{2-} in $PM_{2.5}$ with the SD in the two haze periods. C) Concentration ratio of SO_4^{2-} to OC in the chamber after exposing the water extracts of $PM_{2.5}$ collected in Beijing during the 2018 Haze II event to SO_2 (600 ppb), NO_2 (600 ppb), and NH_3 (80 and 190 ppb) under 90% RH conditions for 2.5 h. D) Molar ratio of SO_4^{2-} to SO_2 as a function of HONO(g) concentration in Beijing during nighttime (16:00–8:00) in the Haze I and Haze II episodes.

collected during the Haze II period to SO_2, NO_2, and NH_3 under 90% RH conditions. As shown in Fig. 5C, a significant increase in the mass ratio of sulfate to OC was observed after exposure, with values of 1.4 ± 0.1 and 1.8 ± 0.02 under 80 and 190 ppb NH_3, respectively, suggesting efficient sulfate formation on the Beijing haze particles. During the exposure process, the reaction rates $k_{NO_2^+HSO_3^-}$ at the two levels of NH_3 are were $3.6 - 6.9 \times 10^8$ M^{-1} s^{-1} (Tables S1 and S2), which are also 3–4 orders of magnitude larger the those for bulk solutions (46, 47) and in good agreement with the kinetics observed from the other seed experiments (Fig. 4), revealing that sulfate formation in the Beijing haze events accelerated at the air–aerosol aqueous interface via Eqs. 1 and 2. As a result, the molar ratio of SO_4^{2-} to SO_2 at nighttime during the two haze episodes exponentially increased with an increasing HONO(g) concentration (Fig. 5D). These field evidences robustly show that the air–aerosol aqueous interface in China winter haze periods are dominated by anions due to the abundant chloride, nitrate, and carboxylic ions (Fig. 5B, Table S3), which accumulate at the air–aerosol aqueous interface and significantly enhance the uptake of NO_2 and subsequent reaction with S(IV) at the aerosol surface. Recently, a few studies proposed that aqueous phase photochemistry including nitrate photolysis and oxalate-Fe(III) photochemistry could promote sulfate formation (48–50). Since those processes all proceed under strong irradiation conditions, which are thus not the cases for this study, because rapid sulfate formation in China haze periods always occurs under very weak solar radiation conditions and even at night (1, 10, 14, 15). Our recent study has compared the different formation pathways of sulfate in Beijing haze periods by using the kinetics of SO_2 oxidation by NO_2 obtained in this work, and found that SO_2 oxidation by NO_2 is the dominant formation pathway for sulfate in Beijing haze while others are relatively unimportant, in part due to low levels of oxidants such as O_3 and H_2O_2 (7). Our current work also revealed that in the reaction process of NO_2 with SO_2, NO_2 is reduced to HONO and the latter subsequently evaporates into the gas phase, which indicates that the aerosol-phase reaction is probably an important source of HONO in haze periods (17). HONO is a major source of OH radicals in the troposphere in some environments, and SO_2 and NOx are abundant in many countries such as China and India. Thus, the enhancing effect of air–aqueous interface anions not only regulates atmospheric aerosol chemistry but also affects atmospheric oxidation capacity, which should be considered in future model simulations and other related studies.

Materials and methods

Laboratory experiments were performed to evaluate SO_2 oxidation by NO_2 on various aerosols under dark conditions by using a home-made 1 m^3 PTFE smog chamber (SI Appendix). To determine the interfacial effects of anions on the sulfate formation, we conducted chamber experiments by consecutively exposing different inorganic and organic particles to SO_2, NO_2, and NH_3 under 90% RH conditions for ~2.5 h and measuring the concentrations of the gas- and aerosol-phase components inside the chamber (see the details in SI Appendix S1) (1, 7, 17). The seeded particles are oxalic acid, NaCl, $(NH_4)_2SO_4$, a NaCl and $(NH_4)_2SO_4$ mixture, sucrose, NH_4NO_3 and water extracts of haze particles from Beijing, which are typical aerosols in Chinese haze periods. Field measurements of gaseous and PM pollutants were performed in Beijing from 2018 December 1 to 2019 January 31, by using the same instruments as those used for the laboratory smog chamber experiments. The sampling site is located on the rooftop (~10 m above the ground) of a three-story building on the campus of the Chinese Research Academy of Environmental Science, which is located in the north part of Beijing city (SI Appendix S2). The pH values of particles inside the chamber and atmospheric $PM_{2.5}$ in Beijing were estimated by utilizing the ISORROPIA-II model (SI Appendix S3). To illustrate difference in distributions of anions and cations at the air–aqueous interface and its effect on SO_2 oxidation by NO_2, we employed a MD model to simulate the ion distribution of Cl^- and Na^+ at the air–water interface of 2.0 M NaCl solution droplets. Moreover, we also performed quantum chemical calculations to investigate the reaction pathway of SO_2 with NO_2 in the aqueous phase (see the details in SI Appendices S3 and S4).

Supplementary Material

Supplementary material is available at *PNAS Nexus* online.

Funding

This work was financially supported by the National Natural Science Foundation of China (nos. 42130704 and U23A2030) and the National Key Research and Development Program of China (2023YFC3706302).

Author Contributions

G.W. conceived and designed the research. S.Z., X.X., S.G., and G.W. conducted the lab chamber experiments. S.Z., S.G., and G.W. analyzed the chamber experiment data. T.Z., H.S., and G.W. performed the theoretical chemistry calculation. J.G., Y.R., and H.L. collected the field samples. C.W. and G.W. analyzed the field observation data. G.W. wrote the paper. Other authors contributed to this work with useful discussions and comments.

Preprints

This manuscript was posted as a preprint at: https://doi.org/10.21203/rs.3.rs-2230064/v1.

Data Availability

The chamber experiments and field observation data are available at https://doi.org/10.5281/zenodo.14898280, while all other data can be found at the Supplementary Material.

References

1 Wang GH, *et al.* 2016. Persistent sulfate formation from London fog to Chinese haze. *Proc Natl Acad Sci U S A.* 113:13630–13635.
2 Seinfeld JH, Pandis SN. *Atmospheric chemistry and physics: from air pollution to climate change.* 2nd ed. John Wiley and Sons, Hoboken, NJ, 2006.
3 Fuzzi S, *et al.* 2015. Particulate matter, air quality and climate: lessons learned and future needs. *Atmos Chem Phys.* 15: 8217–8299.
4 Zhang R, *et al.* 2015. Formation of urban fine particulate matter. *Chem Rev.* 115:3803–3855.
5 Liu T, Clegg SL, Abbatt JPD. 2020. Fast oxidation of sulfur dioxide by hydrogen peroxide in deliquesced aerosol particles. *Proc Natl Acad Sci U S A.* 117:1354–1359.

6 Wang WG, *et al.* 2021. Sulfate formation is dominated by manganese-catalyzed oxidation of SO2 on aerosol surfaces during haze events. *Nat Commun.* 12:1993.

7 Zhang S, *et al.* 2024. Elucidating the mechanism on the transition-metal ion-synergetic-catalyzed oxidation of SO2 with implications for sulfate formation in Beijing Haze. *Environ Sci Technol.* 58:2912–2921.

8 Shao J, *et al.* 2019. Heterogeneous sulfate aerosol formation mechanisms during wintertime Chinese haze events: air quality model assessment using observations of sulfate oxygen isotopes in Beijing. *Atmos Chem Phys.* 19:6107–6123.

9 Wang YX, *et al.* 2014. Enhanced sulfate formation during China's severe winter haze episode in January 2013 missing from current models. *J Geophys Res.* 119:10425–10440.

10 Wang JF, *et al.* 2020. Fast sulfate formation from oxidation of SO2 by NO2 and HONO observed in Beijing haze. *Nat Commun.* 11:2844.

11 Xue J, *et al.* 2019. Efficient control of atmospheric sulfate production based on three formation regimes. *Nat Geosci.* 12:977–982.

12 Tao W, *et al.* 2020. Aerosol pH and chemical regimes of sulfate formation in aerosol water during winter haze in the North China Plain. *Atmos Chem Phys.* 20:11729–11746.

13 Zhang F, *et al.* 2020. An unexpected catalyst dominates formation and radiative forcing of regional haze. *Proc Natl Acad Sci U S A.* 117:3960–3966.

14 Cheng YF, *et al.* 2016. Reactive nitrogen chemistry in aerosol water as a source of sulfate during haze events in China. *Sci Adv.* 2:e1601530.

15 Liu T, Abbatt JPD. 2021. Oxidation of sulfur dioxide by nitrogen dioxide accelerated at the interface of deliquesced aerosol particles. *Nat Chem.* 13:1173–1177.

16 Yao M, *et al.* 2023. Multiphase reactions between organic peroxides and sulfur dioxide in internally mixed inorganic and organic particles: key roles of particle phase separation and acidity. *Environ Sci Technol.* 57:15558–15570.

17 Ge SS, *et al.* 2019. Abundant NH_3 in China enhances atmospheric HONO production by promoting the heterogeneous reaction of SO_2 with NO_2. *Environ Sci Technol.* 53:14339–14347.

18 Li L, Hoffmann MR, Colussi AJ. 2018. Role of nitrogen dioxide in the production of sulfate during Chinese haze-aerosol episodes. *Environ Sci Technol.* 52:2686–2693.

19 Mishra H, *et al.* 2012. Anions dramatically enhance proton transfer through aqueous interfaces. *Proc Natl Acad Sci U S A.* 109: 10228–10232.

20 Zheng G, *et al.* 2020. Multiphase buffer theory explains contrasts in atmospheric aerosol acidity. *Science.* 369:1374–1377.

21 Wang T, *et al.* 2023. Key factors determining the formation of sulfate aerosols through multiphase chemistry—a kinetic modeling study based on Beijing conditions. *J Geophys Res.* 128:e2022JD038382.

22 Bergas-Massó E, *et al.* 2023. Pre-industrial, present and future atmospheric soluble iron deposition and the role of aerosol acidity and oxalate under CMIP6 emissions. *Earths Future.* 11: e2022EF003353. Doi:10.1029/2022EF003353.

23 Ghosal S, *et al.* 2005. Electron spectroscopy of aqueous solution interfaces reveals surface enhancement of halides. *Science.* 307:563–566.

24 Jubb AM, Hua W, Allen HC. 2012. Environmental chemistry at vapor/water interfaces: insights from vibrational sum frequency generation spectroscopy. *Annu Rev Phys Chem.* 63:107–130.

25 Hua W, Verreault D, Allen HC. 2015. Relative order of sulfuric acid, bisulfate, hydronium, and cations at the air-water interface. *J Am Chem Soc.* 137:13920–13926.

26 Hua W, Jubb AM, Allen HC. 2011. Electric field reversal of Na2SO4, (NH4)(2)SO4, and Na2CO3 relative to CaCl2 and NaCl at the air/aqueous interface revealed by heterodyne detected phase-sensitive sum frequency. *J Phys Chem Lett.* 2:2515–2520.

27 Jubb AM, Hua W, Allen HC. 2012. Organization of water and atmospherically relevant ions and solutes: vibrational sum frequency spectroscopy at the vapor/liquid and liquid/solid interfaces. *Acc Chem Res.* 45:110–119.

28 Tobias DJ, Stern AC, Baer MD, Levin Y, Mundy CJ. 2013. Simulation and theory of ions at atmospherically relevant aqueous liquid-air interfaces. *Annu Rev Phys Chem.* 64: 339–359.

29 Wei J, *et al.* 2023. Separating daily 1 km PM2.5 inorganic chemical composition in China since 2000 via deep learning integrating ground, satellite, and model data. *Environ Sci Technol.* 57:18282–18295

30 Wang G, *et al.* 2009. Organic molecular compositions and size distributions of Chinese summer and autumn aerosols from Nanjing: characteristic haze event caused by wheat straw burning. *Environ Sci Technol.* 43:6493–6499.

31 Enami S, Fujii T, Sakamoto Y, Hama T, Kajii Y. 2016. Carboxylate ion availability at the air-water interface. *J Phys Chem A.* 120: 9224–9234.

32 Dalstein L, Chiang K-Y, Wen Y-C. 2023. Surface potential at electrolyte/air interfaces: a quantitative analysis via sum-frequency vibrational spectroscopy. *J Phys Chem B.* 127:4915–4921.

33 Lamoureux G, Roux B. 2003. Modeling induced polarization with classical Drude oscillators: theory and molecular dynamics simulation algorithm. *J Chem Phys.* 119:3025–3039.

34 Knipping EM, *et al.* 2000. Experiments and simulations of ion-enhanced interfacial chemistry on aqueous NaCl aerosols. *Science.* 288:301–306.

35 Tian C, Byrnes SJ, Han H-L, Shen YR. 2011. Surface propensities of atmospherically relevant ions in salt solutions revealed by phase-sensitive sum frequency vibrational spectroscopy. *J Phys Chem Lett.* 2:1946–1949.

36 Jungwirth P, Curtis JE, Tobias DJ. 2003. Polarizability and aqueous solvation of the sulfate dianion. *Chem Phys Lett.* 367:704–710.

37 Hua W, Verreault D, Allen HC. 2014. Surface electric fields of aqueous solutions of NH4NO3, Mg(NO3)(2), NaNO3, and LiNO3: implications for atmospheric aerosol chemistry. *J Phys Chem C.* 118:24941–24949.

38 Mahiuddin S, Minofar B, Borah JM, Das MR, Jungwirth P. 2008. Propensities of oxalic, citric, succinic, and maleic acids for the aqueous solution/vapour interface: surface tension measurements and molecular dynamics simulations. *Chem Phys Lett.* 462:217–221.

39 Enami S, Hoffmann MR, Colussi AJ. 2015. Stepwise oxidation of aqueous dicarboxylic acids by gas-phase OH radicals. *J Phys Chem Lett.* 6:527–534.

40 Finlayson-Pitts BJ, Wingen LM, Sumner AL, Syomin D, Ramazan KA. 2003. The heterogeneous hydrolysis of NO2 in laboratory systems and in outdoor and indoor atmospheres: an integrated mechanism. *Phys Chem Chem Phys.* 5:223–242.

41 Finlayson-Pitts BJ, Pitts JJN. *Chemistry of the upper and lower atmosphere: theory, experiments and applications*. Academic Press, San Diego, CA, 2000.

42 Li L, *et al.* 2018. Formation of HONO from the NH3-promoted hydrolysis of NO2 dimers in the atmosphere. *Proc Natl Acad Sci U S A.* 115:7236–7241.

43 Frisch MJ, *et al. Gaussian 09, Revision A.02*. Gaussian, Inc., Wallingford, CT, 2016.

44 Adamo C, Barone V. 1999. Toward reliable density functional methods without adjustable parameters: the PBE0 model. *J Chem Phys.* 110:6158–6170.

45 Rappoport D, Furche F. 2010. Property-optimized Gaussian basis sets for molecular response calculations. *J Chem Phys*. 133: 134105.

46 Lee Y-N, Schwartz SE. Kinetics of oxidation of aqueous sulfur (IV) by nitrogen dioxide. In: Pruppacher HR, Semonin RG, Slinn WGN, editors. *Precipitation scavenging, dry deposition and resuspension*. Vol. 1. New York: Elsevier, 1983. pp. 453–466.

47 Takeuchi H, Ando M, Kizawa N. 1977. Absorption of nitrogen oxides in aqueous sodium sulfite and bisulfite solutions. *Ind Eng Chem Proc Des Dev*. 16:303–308.

48 Gen M, Zhang R, Huang DD, Li Y, Chan CK. 2019. Heterogeneous SO2 oxidation in sulfate formation by photolysis of particulate nitrate. *Environ Sci Technol Lett*. 6:86–91.

49 Zhang R, Gen M, Huang D, Li Y, Chan CK. 2020. Enhanced sulfate production by nitrate photolysis in the presence of halide ions in atmospheric particles. *Environ Sci Technol*. 54:3831–3839.

50 Zhou Y, *et al*. 2020. Field evidence of Fe-mediated photochemical degradation of oxalate and subsequent sulfate formation observed by single particle mass spectrometry. *Environ Sci Technol*. 54:6562–6574.